AIAA 2003–3212

Computational and Experimental Flow Field Analyses of Separate Flow Chevron Nozzles and Pylon Interaction

Steven J. Massey
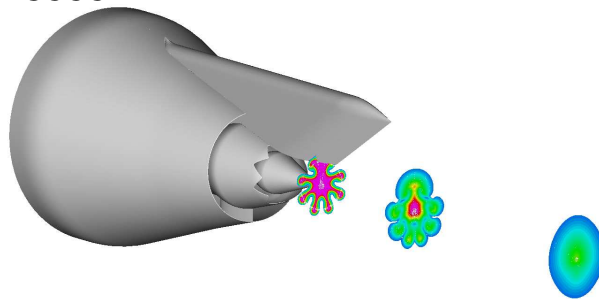*Eagle Aeronautics, Inc., Hampton, VA 23669*

Russell H. Thomas
Aeroacoustics Branch, MS 166, NASA Langley Research Center, Hampton, VA 23681

Khaled S. Abdol-Hamid
Configuration Aerodynamics Branch, MS 499, NASA Langley Research Center, Hampton, VA 23681

Alaa A. Elmiligui
Analytical Services & Materials, Inc., Hampton, VA 23666

9th AIAA/CEAS Aeroacoustics Conference and Exhibit
May 12–14, 2003/Hilton Head, SC

Computational and Experimental Flow Field Analyses of Separate Flow Chevron Nozzles and Pylon Interaction

Steven J. Massey*
Eagle Aeronautics, Inc., Hampton, VA 23669

Russell H. Thomas[†]
Aeroacoustics Branch, MS 166, NASA Langley Research Center, Hampton, VA 23681

Khaled S. Abdol-Hamid[‡]
Configuration Aerodynamics Branch, MS 499, NASA Langley Research Center, Hampton, VA 23681

Alaa A. Elmiligui[§]
Analytical Services & Materials, Inc., Hampton, VA 23666

A computational and experimental flow field analyses of separate flow chevron nozzles is presented. The goal of this study is to identify important flow physics and modeling issues required to provide highly accurate flow field data which will later serve as input to the Jet3D acoustic prediction code. Four configurations are considered: a baseline round nozzle with and without a pylon, and a chevron core nozzle with and without a pylon. The flow is simulated by solving the asymptotically steady, compressible, Reynolds-averaged Navier-Stokes equations using an implicit, up-wind, flux-difference splitting finite volume scheme and standard two-equation $k - \varepsilon$ turbulence model with a linear stress representation and the addition of a eddy viscosity dependence on total temperature gradient normalized by local turbulence length scale. The current CFD results are seen to be in excellent agreement with Jet Noise Lab data and show great improvement over previous computations which did not compensate for enhanced mixing due to high temperature gradients.

Introduction

Typically for modern commercial aircraft, engine installation involves the engine-under-the-wing or the tail mounted configuration. However, even within those two basic categories there are many design variables including structural, aerodynamic, and operational factors. For these standard engine installations and design requirements the industry has highly developed design and analysis processes.[1]

The impact on the net radiated noise of the aircraft is an additional challenge that is emerging as increasingly important in propulsion airframe integration and is the general motivation for the work reported here. One example of an aeroacoustic effect of propulsion airframe integration could be the effect of the pylon on the development of the exhaust plume and on the resulting jet noise. Another area of installation effect on noise is the impact that installation has on noise reduction devices such as chevron nozzles. Many noise reduction devices are studied fundamentally on isolated components. In general, installation effects must be considered because these effects may alter, from the isolated case, the aerodynamic and noise reduction performance of the device or strategy. This focus on both the aerodynamic as well as acoustic interaction effects of installation and propulsion airframe aeroacoustics, will become more important as noise reduction targets become more difficult to achieve.

The work in this paper is a continuation of an on-going effort to study the effect of the pylon on separate flow nozzles including those equipped with the chevron jet noise reduction device. Building on preliminary work,[2] the primary objective of this work is to improve the capability to simulate installed jet configurations and to develop understanding of the characteristics of the flow field of the selected installation configurations through computational solutions compared with flow field experiments performed at the NASA Langley Jet Noise Laboratory. In parallel research, Hunter[3] is developing an installed jet noise prediction method that uses the flow field information from these computational solutions and compares with acoustic experiments that have also been performed at the Jet Noise Laboratory on these same configurations. Together, these three tools are being used to develop an understanding of the acoustic interaction between pylon and chevron nozzles and the more general interaction of pylon and jet with the aim of developing flow and acoustic prediction capability and noise reduction technology for installed jet configurations.

---
*Senior Research Scientist, AIAA Member.
[†]Aerospace Engineer, Senior Member AIAA.
[‡]Aerospace Engineer, Associate Fellow AIAA.
[§]Senior Scientist.

a) Config. 1   b) Config. 6

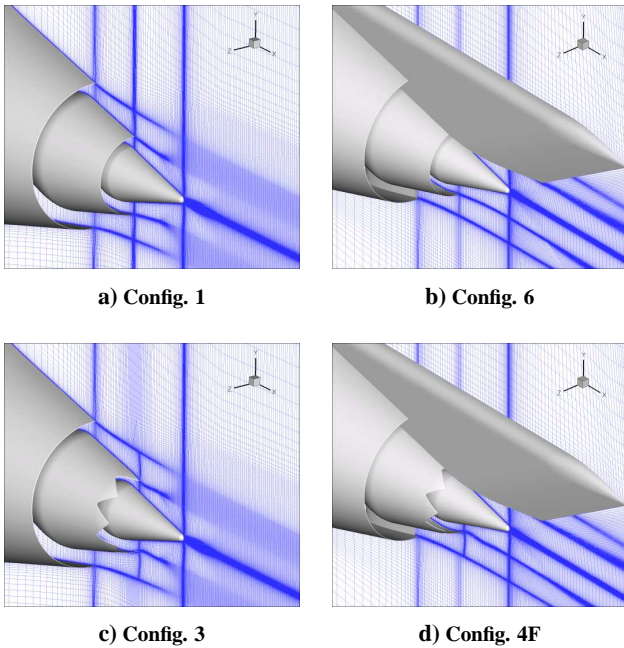c) Config. 3   d) Config. 4F

Fig. 1   Surface and symmetry plane grid lines.

Configurations

The baseline configuration is a separate flow nozzle of bypass ratio of five with an external plug. The nozzle and pylon designs are from a nozzle study performed by Mc-Donnell Douglas (now Boeing) in 1996 and represents a generic design. The chevrons were designed for the core nozzle using guidelines similar to those used in the NASA Advanced Subsonic Transport program. The chevrons are designed to penetrate into the core flow by approximately the thickness of the boundary layer. The trailing edge of the baseline nozzle is chosen to correspond to the mid-point of the chevron axial length. The four configurations analyzed in this study are:

Configuration 1: Baseline round core and fan nozzle with no pylon (Figure 1a).

Configuration 6: Baseline core and fan nozzle with pylon (Figure 1b).

Configuration 3: Eight chevron core nozzle and baseline fan nozzle with no pylon (Figure 1c).

Configuration 4F: Eight chevron core nozzle and baseline fan nozzle with pylon with the tip of a chevron aligned with the pylon (Figure 1d).

The configuration numbering scheme is consistent with previously used configuration numbers.[2] The current configurations 1 and 3 are identical in geometry to the same configurations simulated previously only in this work they are simulated with the results of the improved computational formulation to be described below. The pylon in the current work has a diverging shelf angle of $1.5°$ (configurations 6 and 4F) while the pylon in the previous configurations 2, 4, and 5 had a curved shelf line. The junction in configuration 4F is simply the result of a separate chevron

and pylon design combined with no added design feature for the junction similar to the junction in the previous configuration 4.

Experimental Flow Conditions

Surveys of the flow fields of configurations 1, 3, and 4F are used to compare with the results of the simulations in subsequent sections. The surveys were performed in the NASA Langley Low Speed Aeroacoustic Wind Tunnel with a traverse apparatus moving a single rake of probes (see Figure 2). Mean total pressure and total temperature were measured with a rake that was populated with three total pressure and three total temperature probes and traversed in cross-sectional planes at $x/D = 2$, 5, 10, and 17. At each cross-section a grid was mapped with measurements taken typically in 0.64 cm increments at $x/D = 2$ and 5 and in 1.27 cm increments at $x/D = 10$ and 17. The grids were sized at each axial station to cover most of the core and the fan plume. As a result, several hundred increments and samples were taken in order to complete a survey at a single axial station. Maintaining the core and fan jet operating condition was critical to obtaining a good survey. Table 1 lists the mean values of the core and fan operating conditions and the standard deviation of those conditions for a typical survey at a single axial station, indicating that the operating conditions were in fact maintained well over the more than an hour of run time required for each axial station.

Table 1   Mean and standard deviation values for the core and fan operating conditions during the survey of configuration 3 at $x/D = 5$.

	Mean	Standard Dev.
NPR Core	1.557	0.004
T_t Core	826.1 K	3.3 K
NPR Fan	1.747	0.005
T_t Fan	358.7 K	0.8 K

Computational Flow Conditions

The flow conditions for both experiments and computations are set at the take-off cycle point. The free stream Mach number is 0.28 with total pressure and temperature set to standard atmospheric conditions at sea level of 101353 Pa and 295 K respectively. The fan pressure ratio is 1.75 with total temperature of 359 K. The core pressure ratio is 1.56 with total temperature of 828 K.

Numerical Method

The fluid flow is simulated by solving the asymptotically steady, compressible, Reynolds-averaged Navier-Stokes equations using an implicit, up-wind, flux-difference splitting finite volume scheme and standard two equation k-ε turbulence model[4] with a linear stress representation and the addition of an eddy viscosity dependence on total temperature gradient through the variation the C_μ closure coefficient, see Abdol-Hamid et $al.$[5] All computations are performed using the parallel, multiblock, structured grid code
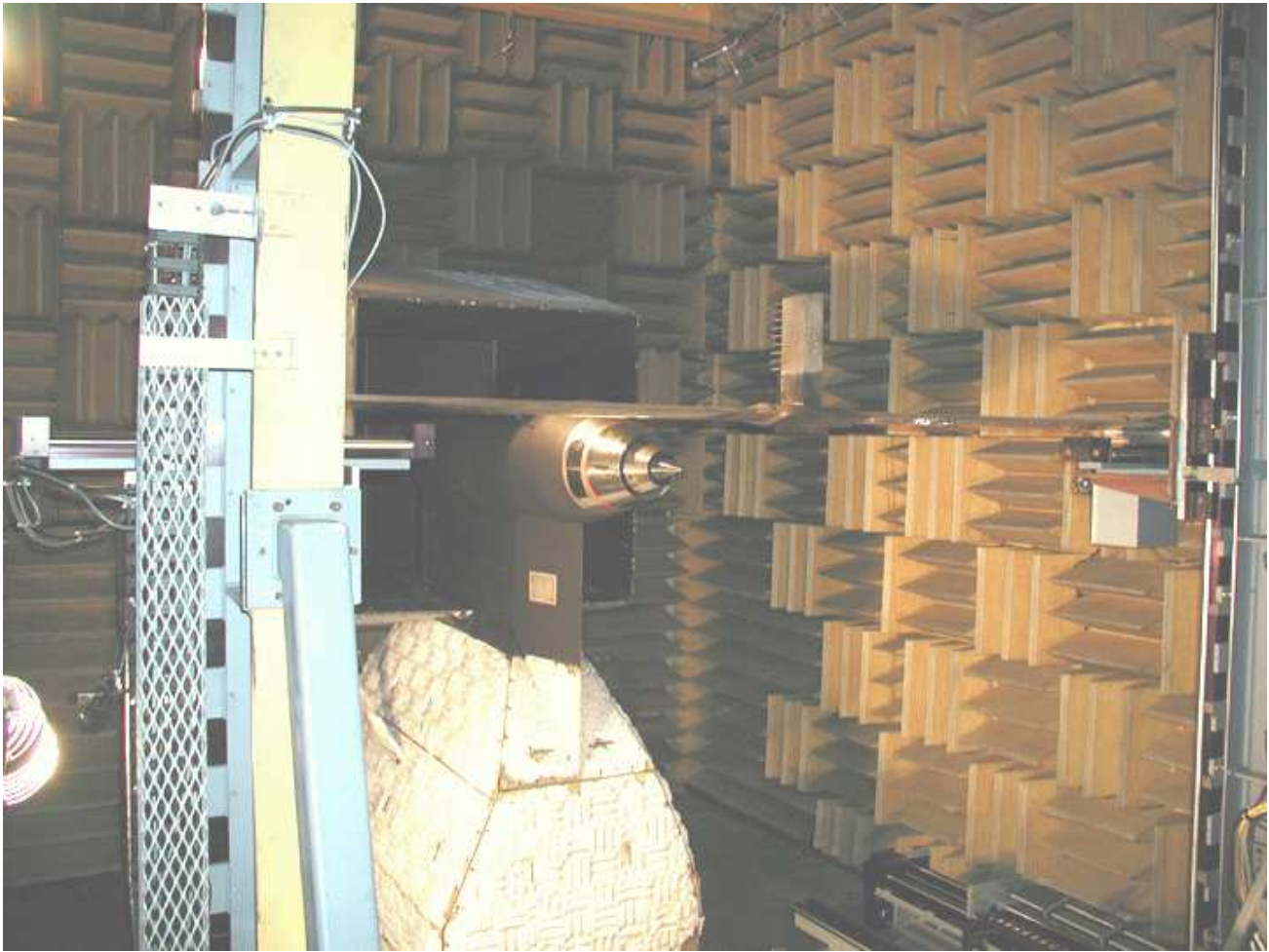
Fig. 2 Photograph, looking upstream, of the flow field survey experiment in the NASA Langley Low Speed Aeroacoustic Wind Tunnel. Configuration 1 is installed on the jet engine simulator surrounded by the wind tunnel nozzle. Rake of probes (center of photo) is seen mounted on a traverse mechanism.

PAB3D.[6] Viscous diffusion terms are modeled as uncoupled in the flow direction and fully coupled in the crossflow direction and a 3-factor scheme is used for the approximation of implicit terms.

Grid sequencing is used to accelerate convergence by solving 1/4 then 1/2 of the grid in each of the three computational directions. The general solution procedure followed is to solve the region near the nozzle via time marching, then solve the plume blocks via space marching, then finally run at least 200 time marching iterations on just the plume blocks and adjacent upstream blocks in order to smooth any inflections at the time/space marching block boundary. Typical iteration counts for 3-D grids at each grid level are 5,000, 4,000, 3,000 and 2,000. Axisymmetric cases are stiffer and require 10,000 iterations per grid level. A sample convergence history, Figure 3, in terms of flow and turbulence residual is shown for four grid sequence levels, where 0.5 denotes half of the spacing used for the production runs. Converged solutions for centerline total temperature, shown in Figure 4, are essentially identical at all grid levels and demonstrate numerical verification for the axial and radial directions. Consistency between the axisymmetric solutions and the periodic solutions of the

chevron nozzle without pylon provide confidence that the azimuthal direction is also fully resolved with 40 cells per chevron or $1.125°$ resolution. Grid sizes range from less than 300,000 cells for a $6°$- two cell wedge grid to over 16 million cells for the full $180°$ chevron/pylon grid, see Table 2 and Figure 1. All surfaces are gridded and run as viscous with the exception of the lower bifurcator and a very small tip region of the plug. The average value of the law of the wall coordinate, y^+, of the first cell center is approximately one with a minimum of 0.4 and a maximum of five. The solution domain extends over six core diameters, ($D = 12.8$ cm) upstream of the fan exit, nearly 32 D downstream and six D radially. In all plots, the origin of the x-axis, $x/D = 0.0$, is set to the fan nozzle exit, which puts the core exit at $x/D = 0.83$ and the plug tip at $x/D = 1.87$.

Typical run times for the fully converged solution at the fine grid level are less than 40 hours for 16.2 million cells using up to 21 2-GHz Pentium 4 nodes on an unbalanced grid. Balanced computations using 8 CPU's for the eight plume blocks containing 600,000 cells each, yield parallel efficiencies of up to 97% or a speed up factor of 7.8.
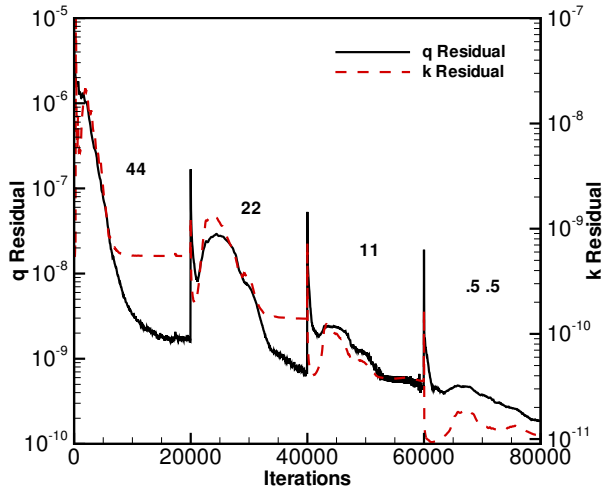
Fig. 3 Config. 1-axi, Round Nozzle: Residual history at four levels of grid refinement.
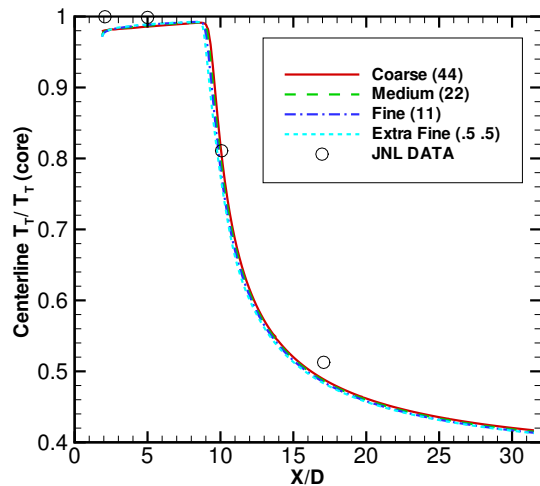

Fig. 4 Config. 1-axi, Round Nozzle: Centerline total temperature at four levels of grid refinement.

Table 2 Zonal grid cell counts. *Config. 1-axi is axisymmetric and fully time marched.

| | Time Marched | Space Marched | |
Config.	$x/D \leq 14$	$x/D > 14$	Total
$1 - axi^*$	2 x 148,464		2 x 148,464
1	4,083,072	1,797,120	5,880,192
6	7,805,440	3,594,240	11,399,680
3	10,125,312	3,594,240	13,719,552
4F	12,620,096	3,594,240	16,214,336

Modified $k - \varepsilon$ Model

The $k - \varepsilon$ model is the most popular two-equation turbulence model and is widely used across many flow regimes, even though it was developed and tuned primarily for two-dimensional, incompressible flows. Thus, it is suspected that observed errors in resolving high temperature jet mixing is a result of the model being applied outside of its envelope. The physical mechanism for the missing quantity of turbulent mixing is thought to be due to the absence of the density contribution to the Kelvin-Helmholtz instability. Experimentally[7,8] it has been shown that the spatial growth of a two-dimensional shear layer is proportional to the square root of the density ratio of the two mixing fluids. In a recent study by Tam and Ganesan,[9] a density based correction was applied on top of the Thies and Tam[10] modified $k - \varepsilon$ model, however it is strictly intended for free shear flows and therefore not applicable to the current configurations. With installed jets it is particularly important that the model apply to both free shear and wall bounded flows. For the purpose of the present study, a minimally invasive correction only to turbulent eddy viscosity is used to rectify the mixing deficiency for high temperature jets. To insure that the modified $k - \varepsilon$ model returns to the original model for cold jets and that it remains accurate for wall bounded flows, turbulence scaled total temperature, $\bar{T}$, is chosen as the variable for the additional eddy viscosity dependence, where

$$\bar{T} = \frac{k^{3/2}}{\varepsilon} \frac{\|\nabla T_t\|}{T_t}. \tag{1}$$

The functional relationship was determined by the best match to experimental data for the baseline round nozzle and is as follows,

$$C_\mu = C_{\mu 0} \left[1 + \frac{C_T \bar{T}^3}{1 + C_M M_t^2} \right] \tag{2}$$

where the standard $k - \varepsilon$ closure coefficient is $C_{\mu 0} = 0.09$. The temperature gradient coefficient, C_T, is set to 24.33 by best fit to data after assigning the turbulence Mach number coefficient, C_M to 4. Turbulence Mach number, M_t, is defined by

$$M_t^2 = 2k/a^2 \tag{3}$$

where a is the speed of sound. For this study no attempt was made to construct a general functional dependence on turbulence Mach number, hence Eq. 2 should only be used for subsonic jet flows. However, this has now been successfully addressed in Abdol-Hamid *et al.*[5]

Results

The three issues to be addressed in this section are as follows; 1) the rectified CFD results using the modified $k - \varepsilon$ model versus the original CFD results, 2) the validation of CFD results with experimental data, and 3) explanation of the physical characteristics of the flows.
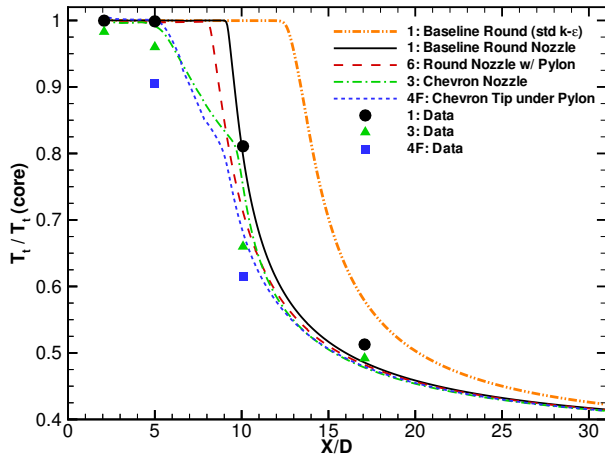
Fig. 5   Total temperature along jet axis.

CFD Rectification

The effect of the temperature gradient modified $k - \varepsilon$ model over the standard $k - \varepsilon$ model for the round nozzle is to increase turbulent mixing and hence decrease the potential core length by 3.4 core diameters, D. The core lengths are tabulated in Table 3 and are defined for the x/D in which $T_t = 0.995 T_{t_\infty}$ along the axis of the jet, see Figure 5. The action of the modified $k - \varepsilon$ model in terms

Table 3   CFD Potential Core Length

Config.	Core length, D
1-std $k - \varepsilon$	12.5
1-mod $k - \varepsilon$	9.1
6	8.1
3	4.6
4F	5.4

of the increased eddy viscosity closure coefficient is shown in Figure 6, where the *ratio* of the actual to the standard value of 0.09 is plotted. In the code, the maximum ratio is set to 5, however, most of the flow fields are well below 3. As a result of the undisturbed shear layers, which create strong temperature gradients, the round jet configuration exhibits the highest amount of C_μ amplification. CFD solutions of the general flow field are depicted for the round nozzle, Figures 7-10, with the standard $k - \varepsilon$ model followed by all configurations with the modified $k - \varepsilon$ model. Note, for configuration 3., the symmetry plane was plotted for the solution rotated by 22.5° to be consistent with experimental crossflow plots.

CFD Validation

As previously discussed, the present model was tuned on the axisymmetric grid to the round nozzle experimental results. Particular attention was paid to matching the axial total temperature at $x/D = 5$ and 10. The model was then frozen for the other cases. Computed total temperature along the axis is plotted with experimental data in Figure 5. Comparing the data points at x/D of 5 and 10, configuration 1 is on data, configuration 3 is less than 1
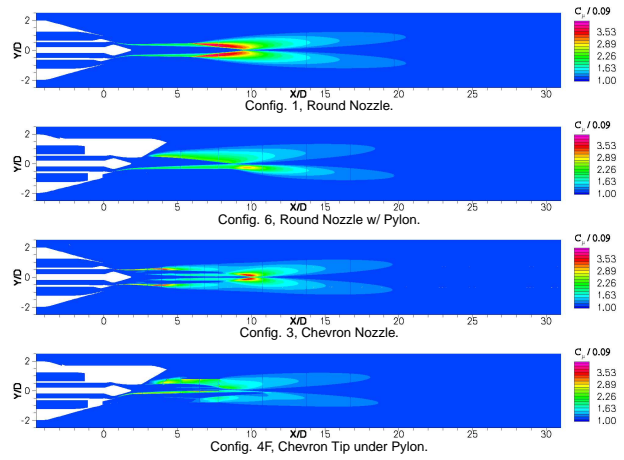

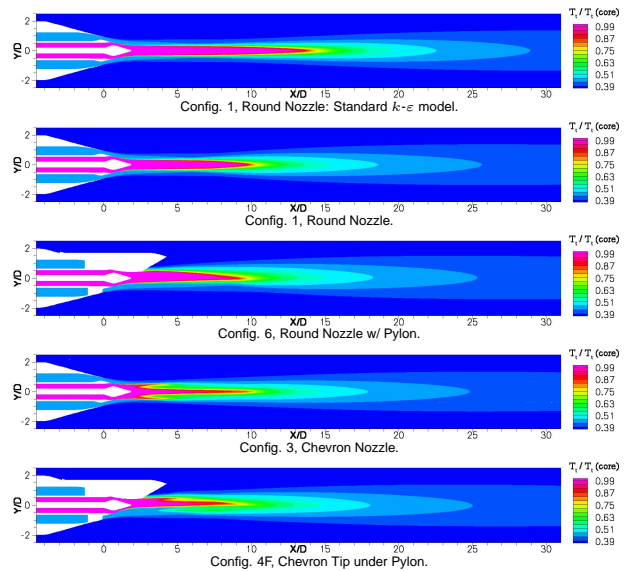**Fig. 6   CFD: C_μ factor on symmetry plane.**

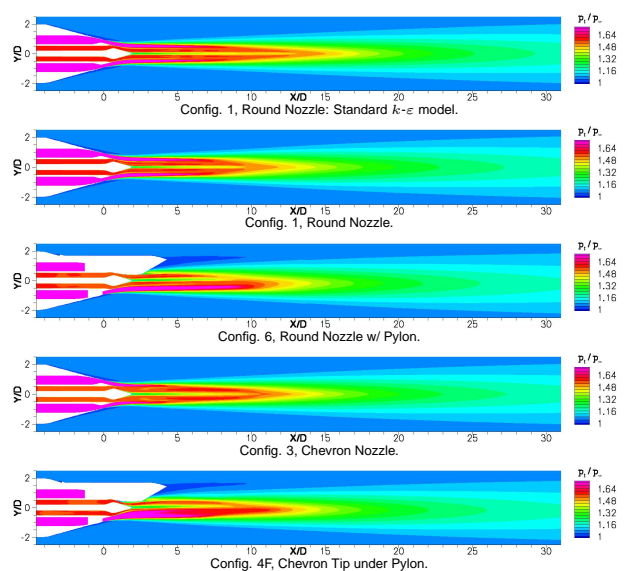**Fig. 7   CFD: Total temperature on symmetry plane.**

Fig. 8   CFD: Total pressure on symmetry plane.
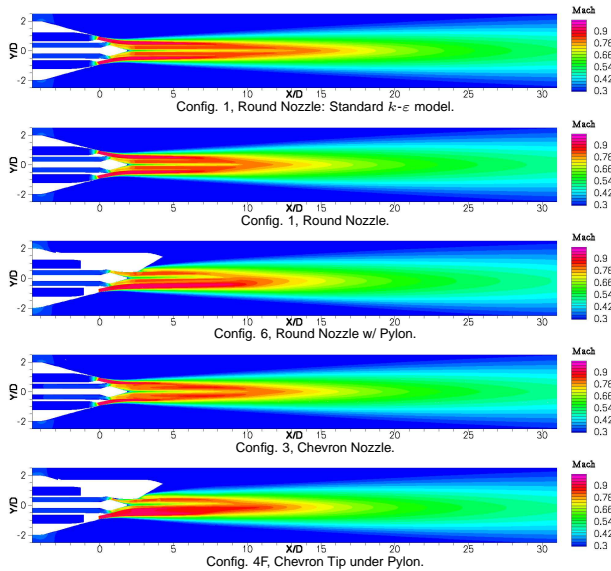
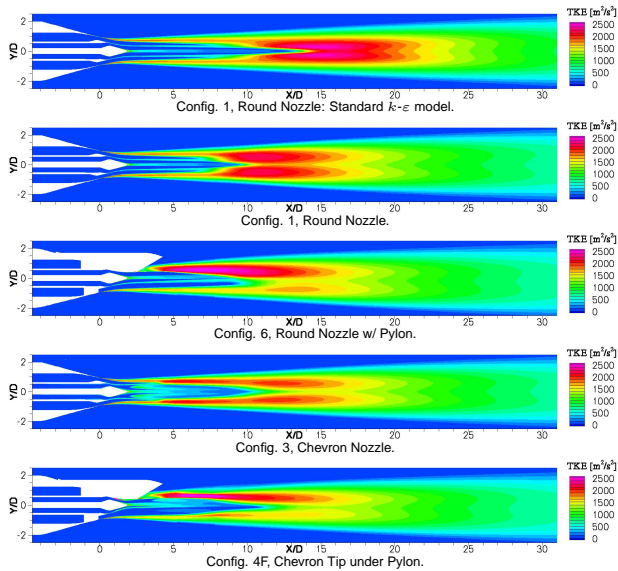**Fig. 9   CFD: Mach number on symmetry plane.**

Fig. 10   CFD: Turbulent kinetic energy on symmetry plane.

D under mixed, and configuration 4F is between 1 and 2 D under mixed. Relative errors compared to the predicted round core length are less than 11% for configuration 3 and 11% to 22% for configuration 4F.

In comparisons with crossectional data for total temperature and pressure, see Figures 11 - 17, the thickness and shape of the shear layers are seen to be in excellent to good agreement with measured data. Note, no experimental data was taken for configuration 6. Also, for configuration 3. the CFD solution was rotated in the azimuthal direction by $22.5°$ to align it with the experimental data. For the total temperature plots, the contour range extends from 0.39 to 0.99 with a level spacing, ΔT_t, of 0.04. For total pressure, the range is from 1.00 to 1.72 with spacing of $\Delta p_t = 0.04$. In the experimental data plots, the data points were taken at Δx and $\Delta y = 0.1D$ intervals and are marked with a small black dot. This tends to smear out thin shear layers, but does not account for the mismatch with CFD, which is

a result of the under prediction of mixing. For configuration 1, T_t is in near perfect agreement and p_t is within one contour level of agreement, see Figures 11 and 12. For configuration 3 shown in Figures 14 and 15, the mixing lobes total temperature and pressure differ by only two contour levels. With the addition of the pylon, configuration 4F shows a slightly larger deviation from measured data, see Figures 16 and 17. Focusing on the chevron induced crossflow plumes at $x/D = 5$, T_t is two to four levels off, with the highest difference being in a small region near the lower bifurcator. The higher than expected temperature near the lower bifurcator is likely a result of not modeling it as a viscous surface, hence there is a lower level of turbulent mixing in this region. For total pressure, the contours are again seen to be two levels higher than measured. The percent error in terms of the contour range is summarized in Table 4. Calculated mass flow is also in good agreement with measured data, see Table 5. Experimentally, there was some discrepancy between two methods of measurement of up to 0.36 kg/sec, however, in both sets of measurements the trend was the same, so the comparison of normalized values is valid and in excellent agreement with CFD.

Table 4   Relative CFD Crossflow Error

Config.	T_t Error	p_t Error
1	$\approx 0\%$	$< 5.5\%$
3	12.0%	11.0%
4F	12.0-24.0%	11.0%

Table 5   Mass flow Comparison. ***Config. 6 was estimated based on area ratio.**

Config.	$\frac{CFD}{7.835 kg/s}$	$\frac{Exp.}{7.902 kg/s}$	Error
1	1.000	1.000	0%
6	0.940	0.94^*	0%
3	0.993	0.994	-0.1%
4F	0.939	0.936	0.3%

Flow Physics

The purpose of creating a chevron core nozzle is to enhance mixing and hence reduce noise with very little thrust loss. Preliminary calculations for the current chevron nozzles show a thrust loss of less than one percent. To clearly show the mixing effects of the chevron core and the pylon, a non-dimensionalized, mass averaged turbulence kinetic energy and total temperature expressions are introduced, shown in Figures 18 and 19 respectively. The expressions follow those published by Kenzakowski *et al.*[11] and are defined as follows:

$$\hat{k} = \frac{\int_A \sqrt{\frac{k}{q}} \rho u \, dA}{\int_A \rho u \, dA} \tag{4}$$

$$\hat{T}_t = \frac{\int_A \phi \rho u \, dA}{\int_A \rho u \, dA} \tag{5}$$

Fig. 11 Config. 1, Round Nozzle: Total temperature cross sections at x/D of 2, 5, 10 and 17.
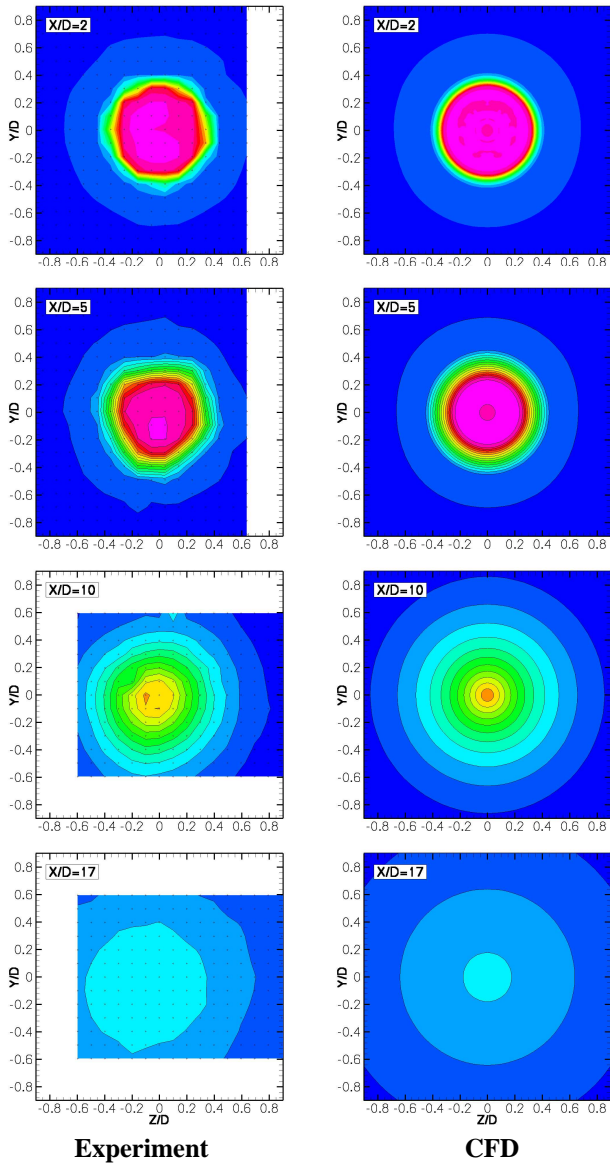

Fig. 12 Config. 1, Round Nozzle: Total pressure cross sections at x/D of 2, 5, 10 and 17.

where

$$\phi = \frac{T_t - T_{t_{FAN}}}{T_{t_{CORE}} - T_{t_{FAN}}} \quad (6)$$

with integration only performed over areas where

$$0.005 \leq \phi \leq 1. \quad (7)$$

From the figures it is clear that the introduction of the chevron core nozzle greatly enhances turbulent mixing, while the pylon installation contributes to the mixing by only a small amount for the round nozzle and even less for the chevron nozzle. Chevrons are seen to be an excellent method to enhance mixing without introducing much turbulence in the near-field compared to the round nozzle with pylon and actually reducing it in the far-field, see Figure 18.

The mechanism for the enhanced mixing due to both pylon and chevrons can be seen by examining the cross-

flow velocity vectors at $x/D = 2$, shown in Figure 20. In these plots, uniformly spaced vectors were plotted with the length proportional to the magnitude over contours of the axial velocity component, u. In both cases, as the pylon and plug close out, the crossflow velocity vectors show flow moving in the direction to fill in the wake. For the round nozzle without a pylon, an overall inward flow is observed due to the secondary flow set up by the plug. With the addition of the pylon in configuration 6, a stronger overall vertical flow toward the pylon is setup. Also, because the pylon is also tapered in the horizontal direction, an additional horizontal velocity is induced. This flow then separates at the sharp bottom edge of the pylon and rolls up into a small vortex. For the chevron nozzle without a pylon, configuration 3, an octagonal shaped influence on the plug flow at the jet center is seen in the crossflow as well
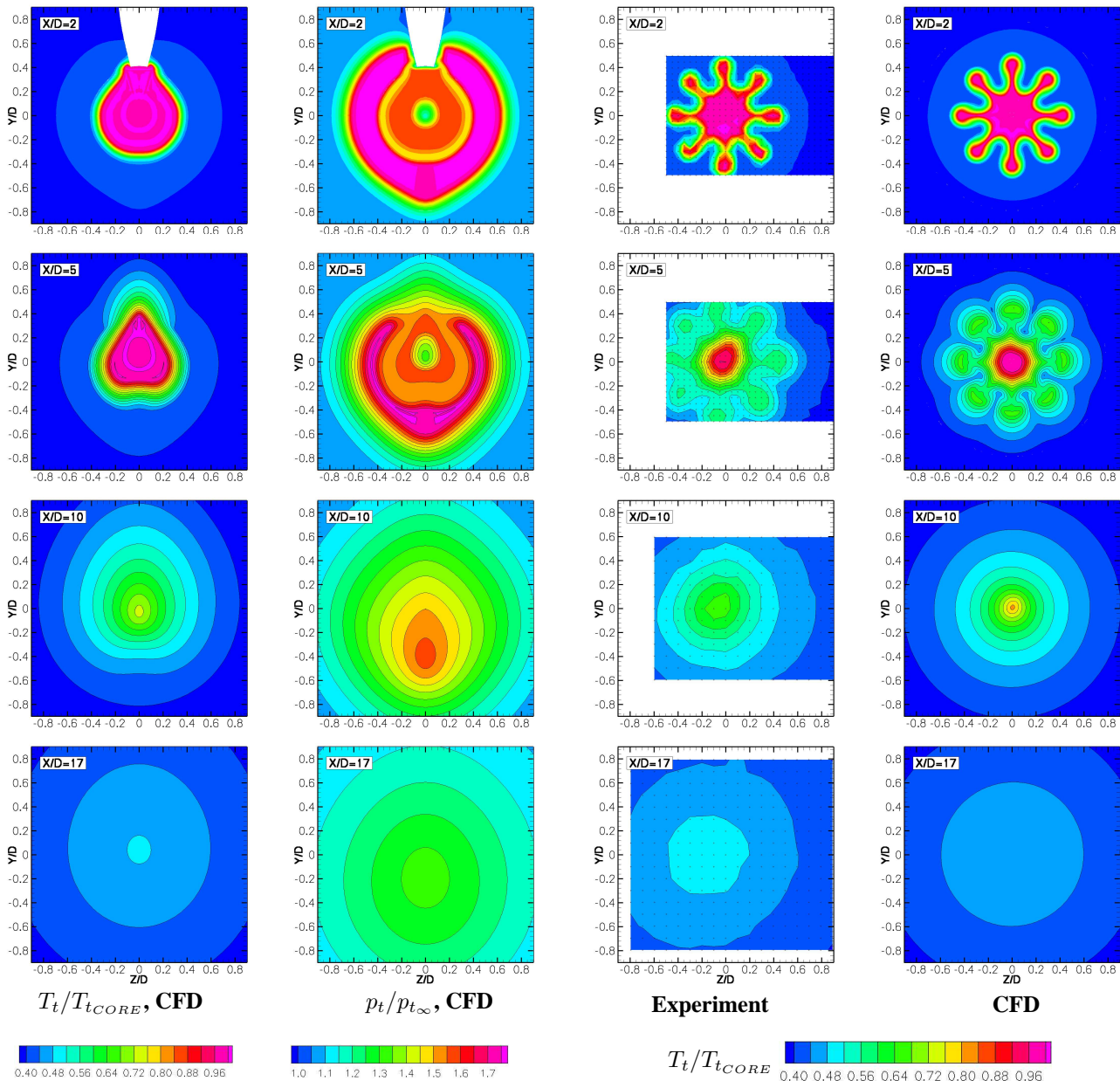
Fig. 13 Config. 6, Round Nozzle w/ Pylon: Total temperature and pressure sections at x/D of 2, 5, 10 and 17.

Fig. 14 Config. 3, Chevron Nozzle: Total temperature cross sections at x/D of 2, 5, 10 and 17.

as the axial flow. However, the strongest effect by far is on the core/fan interface. Note, in this figure, configuration 3 has not been rotated as in the previous plots, therefore its chevrons are oriented as shown in Figure 1c, and are aligned with configuration 4F, where the chevron tip is at the $z/D = 0$. It is observed that the chevrons allow the core flow to stream out in a strong crossflow plume much like a mushroom cloud, where the hot core flow rushes up while drawing the cooler flow down around its base. When the effect of the pylon is added in for configuration 4F, two notable effects are observed; 1) because of the pylon blockage, no fan flow can be drawn down near the pylon, and 2) the vortex on the crossflow plume adjacent to the pylon constructively interferes with the separation vortex coming from the bottom edge of the pylon and forms a much stronger vortex than in configuration 6. Since this vortex
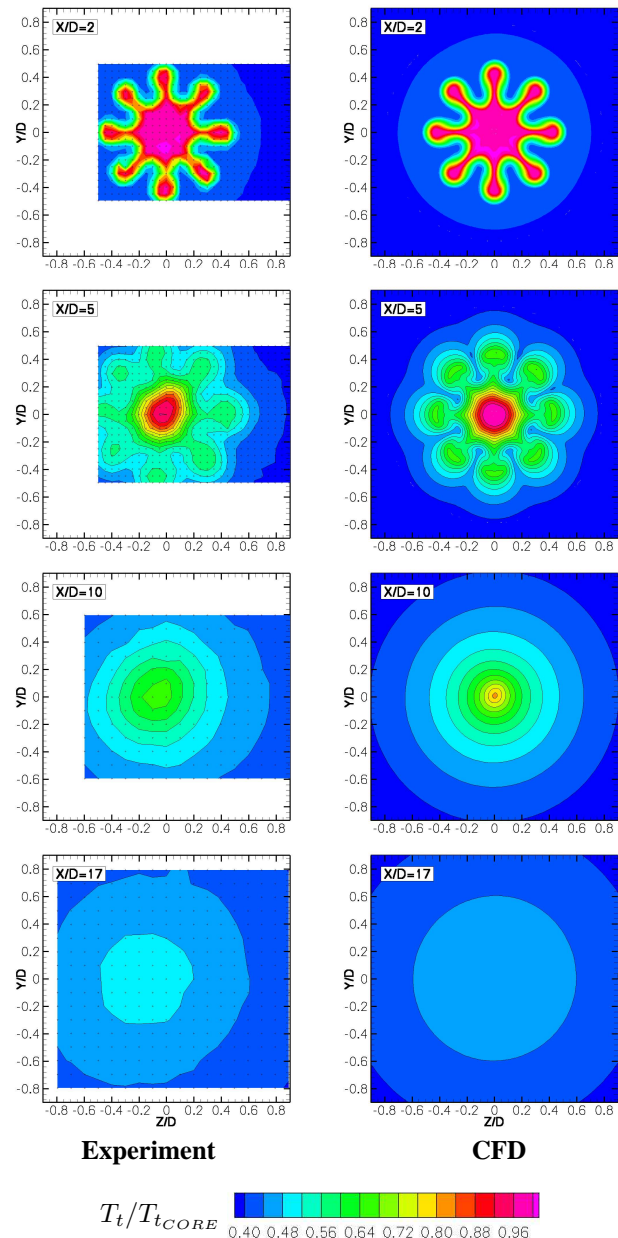
carries turbulence energy[2] from both the boundary layer of the pylon as well as the core/fan shear layer, it is expected to be an additional source of noise.

Concluding Remarks

The purpose of this study was to provide insight into the flow physics of pylon-jet interactions and to provide the input mean flow field to acoustic prediction methods for installed jet noise. Important flow phenomenon were identified and the modeling techniques required to provide highly accurate mean flow field data specifically for use as input to acoustic prediction models were established. Four configurations were considered; a baseline round nozzle with and without a pylon, and a chevron core nozzle with and without a pylon. The flow was simulated by solving the asymptotically steady, compressible, Reynolds-averaged
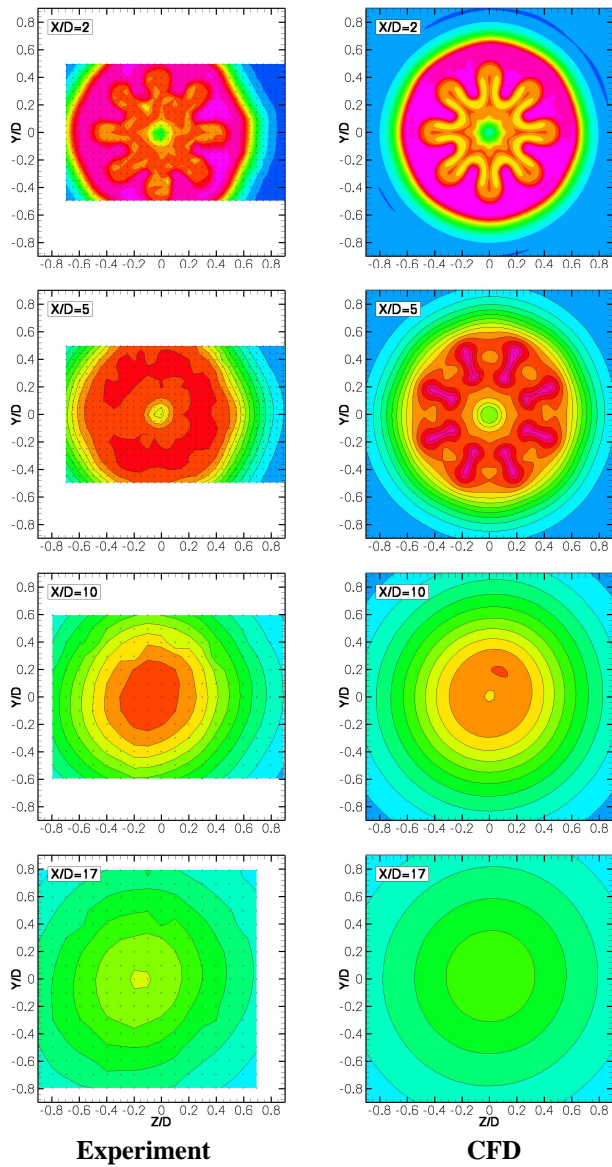
Fig. 15   Config. 3, Chevron Nozzle: Total pressure cross sections at x/D **of 2, 5, 10 and 17.**

Fig. 16   Config. 4F, Chevron Tip under Pylon: Total temperature cross sections at x/D **of 2, 5, 10 and 17.**

Navier-Stokes equations with a temperature gradient modified two-equation $k-\varepsilon$ turbulence model. The current CFD results are seen to be in good to excellent agreement with Jet Noise Lab data and show great improvement over previous computations which did not compensate for enhanced mixing due to high temperature gradients. In terms of the potential core length, which is the clearest single indicator of error, the new round nozzle computations are in complete agreement with experimental data. This is in sharp contrast to initial computations using the unmodified $k-\varepsilon$ model, which over predicted potential core length by 3.4 core diameters or 37%. Current results for the chevron core nozzle without the pylon show a potential core length error of less than one core diameter. The inclusion of the pylon increases the error to between one and two core diameters. Relative to the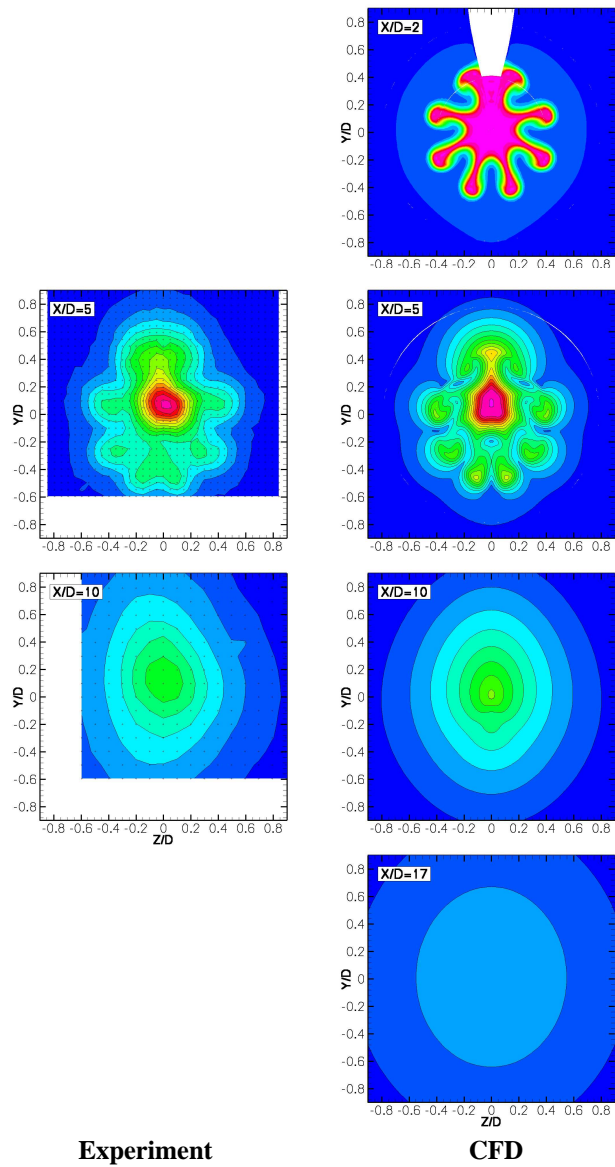 round nozzle core length, these errors are less than 11% for configuration 3 and 11% to 22% for configuration 4F. This study has also clearly shown that installation effects are significant and introduce local and global changes to the flow. Of critical importance is the interface between the chevron induced vortical flow and the bottom edge of the pylon which in the configuration 4F interferes constructively to produce a potential source of noise. With a firm understanding of the flow physics and robust numerical model, future research will aim to design more affective noise attenuating nozzle modifications, while further refining CFD prediction capabilities.
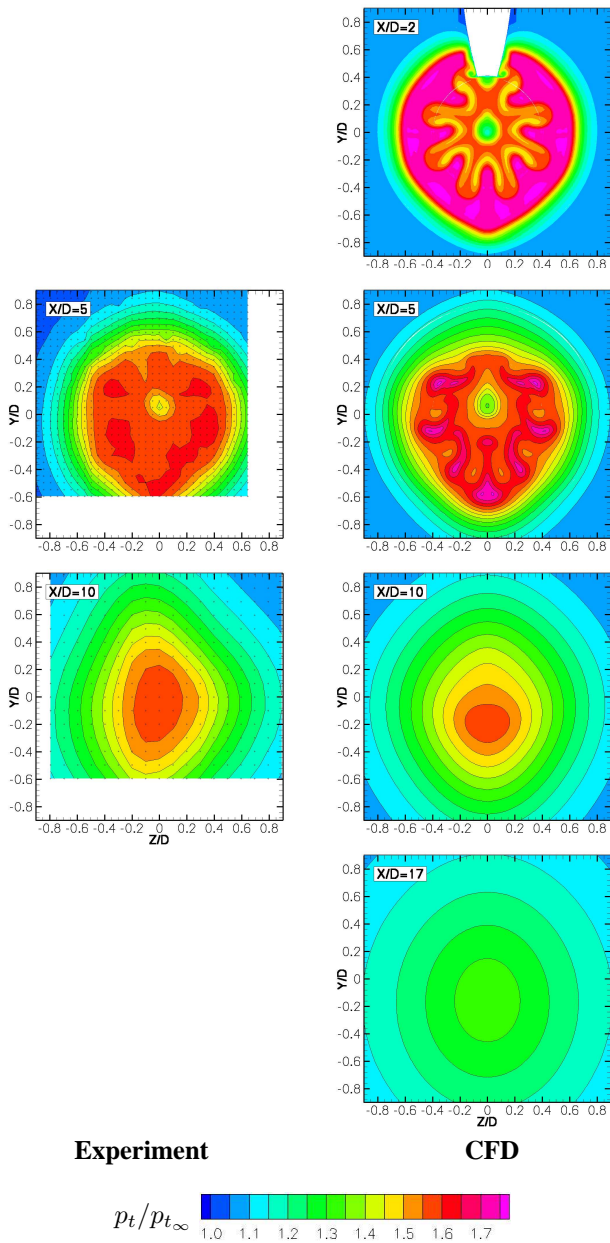
Acknowledgments

Fig. 17 Config. 4F, Chevron Tip under Pylon: Total pressure cross sections at x/D of 2, 5, 10 and 17.

the Configuration Aerodynamics Branch of NASA Langley Research Center for their many helpful discussions and Mike Wiese of NASA-LaRC/AS&M Geolab for all grid construction. This research was funded by NASA-LaRC.

References

[1]Early, K., "Propulsion Airframe Integration Design, Analysis and Challenges Going Into the 21st Century," Paper No. 6103, 2000, Presented at the International Council of the Aeronautical Sciences.

[2]Thomas, R. H., Kinzie, K. W., and Pao, S. P., "Computational Analysis of a Pylon-Chevron Core Nozzle Interaction," AIAA Paper 2001-2185, 2001.

[3]Hunter, C. A. and Thomas, R. H., "Development of a Jet Noise Prediction Method for Installed Jet Configurations," AIAA Paper 2003-3169, 2003.

[4]Jones, W. P. and Launder, B. E., "The Prediction of Laminarization with a Two-Equation Model of Turbulence," *Int. J. Heat Mass Transf.*, Vol. 15, 1972, pp. 301–314.
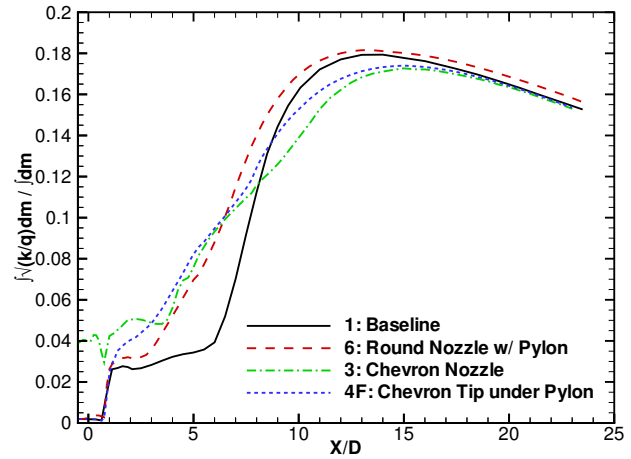
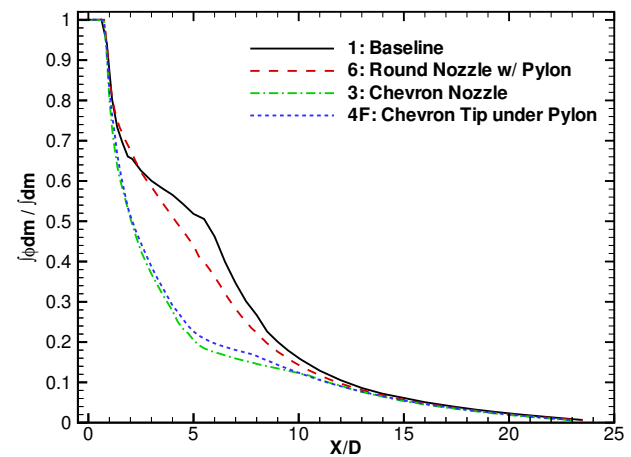Fig. 18 Mass averaged, non-dimensional turbulence intensity.

Fig. 19 Mass averaged, non-dimensional total temperature.

[5]Abdol-Hamid, K. S., Pao, S. P., Massey, S. J., and Elmiligui, A. A., "Temperature Corrected Turbulence Model for High Temperature Jet Flow," AIAA Paper 2003-4070, 2003.

[6]Abdol-Hamid, K. S., "Development of Three-Dimensional Code for the Analysis of Jet Mixing Problem," NASA CR 4200, 1988.

[7]Dimotakis, P. E., "Two-Dimensional Shear-Layer Entrainment," *AIAA Journal*, Vol. 24, No. 11, 1986, pp. 1791–1796.

[8]Brown, G. and Roshko, A., "On density effects and large structure in turbulent mixing layers," *J. Fluid Mech.*, Vol. 64, 1974, pp. 775–816.

[9]Tam, C. and Ganesan, A., "A Modified $k - \varepsilon$ Turbulence Model for Calculating the Mean Flow and Noise of Hot Jets," AIAA Paper 2003-1064, 2003.

[10]Thies, A. T. and Tam, C. K. W., "Computation of Turbulent Axisymmetric and Nonaxisymmetric Jet Flows Using the k-ε Model," *AIAA Journal*, Vol. 34, No. 2, 1996, pp. 309–316.
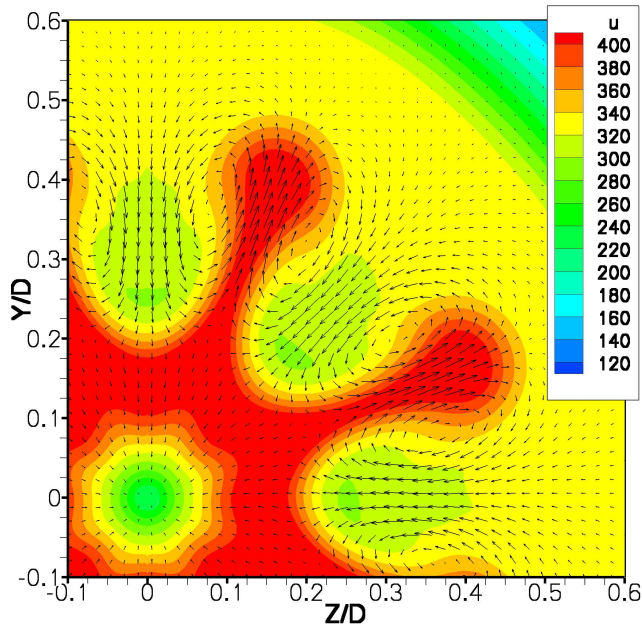
[11]Kenzakowski, D. C., Shipman, J., and Dash, S. M., "Turbulence Model Study of Laboratory Jets with Mixing Enhancements for Noise Reduction," AIAA Paper 2000-0219, 2000.
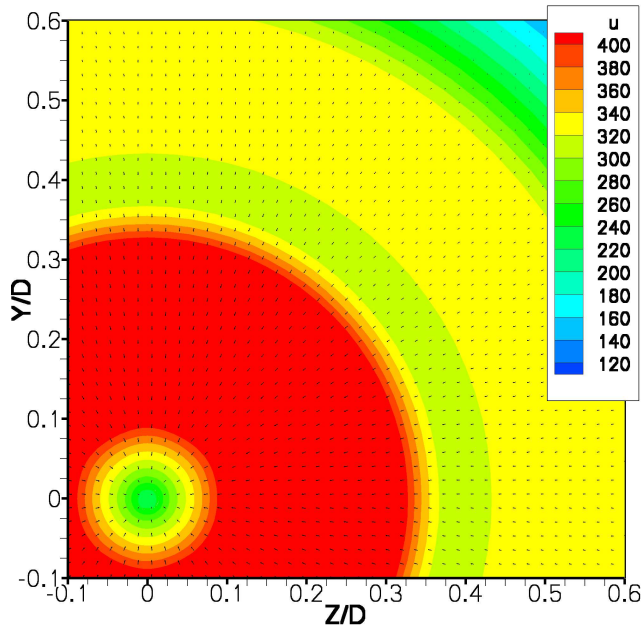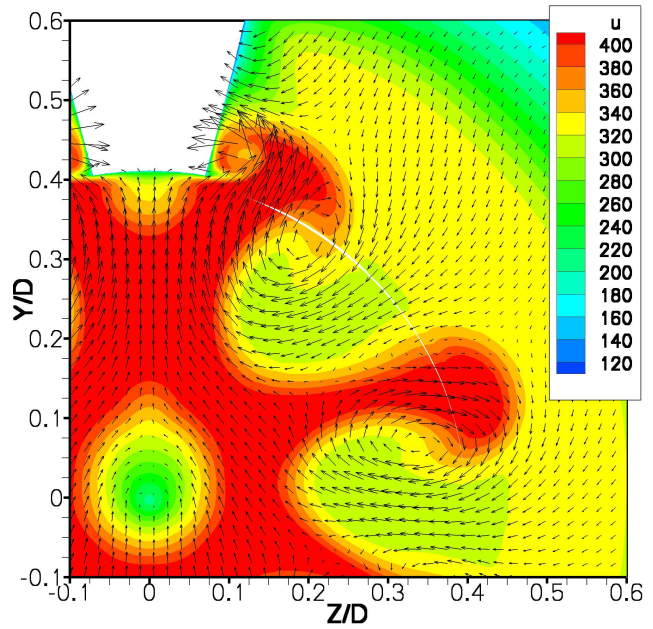
a) Config. 1, Round Nozzle.
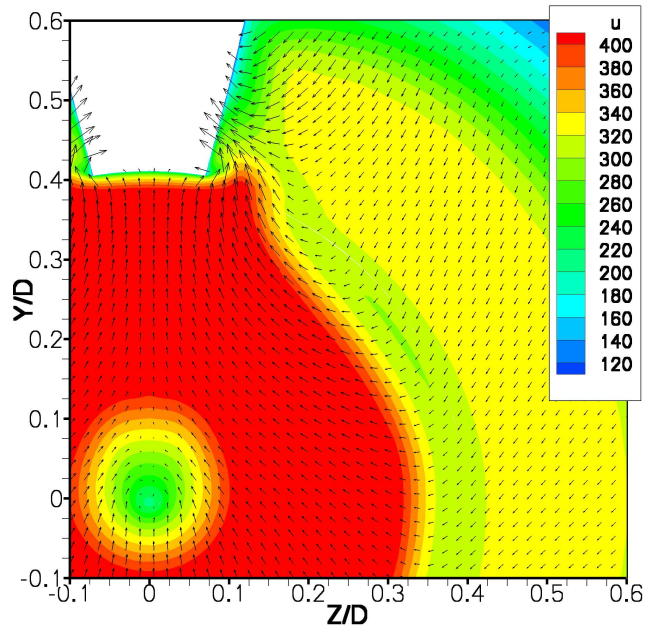
b) Config. 6, Round Nozzle w/ Pylon.

c) Config. 3, Chevron Nozzle.

d) Config. 4F, Chevron Tip under Pylon.

Fig. 20   Crossectional velocity vectors with contours of u [m/s] at x/D of 2.